HTML ABSTRACT + LINKS

Diffraction effects in optical interferometric displacement detection in nanoelectromechanical systems

T. Kouh, D. Karabacak, D. H. Kim,[a] and K. L. Ekinci[b]
Department of Aerospace and Mechanical Engineering, Boston University, Boston, Massachusetts 02215

(Received 5 August 2004; accepted 12 November 2004; published online 27 December 2004)

Optical interferometric displacement detection techniques have recently found use in the study of nanoelectromechanical systems (NEMS). Here, we study the effectiveness of these techniques as the relevant NEMS dimensions are reduced beyond the optical wavelength used. We first demonstrate that *optical cavities* formed in the sacrificial gaps of subwavelength NEMS enable enhanced displacement detection sensitivity. In a second set of measurements, we show that the displacement sensitivity of *conventional* path-stabilized Michelson interferometry degrades rapidly beyond the diffraction limit. Both experiments are consistent with numerical models. © *2005 American Institute of Physics*. [DOI: 10.1063/1.1843289]

Recently, a great deal of experimental[1,2] and theoretical[3] interest has been directed towards submicron resonant mechanical devices. These nanoelectromechanical systems (NEMS) possess extremely high operation frequencies, minuscule active masses, very small force constants and high quality (Q) factors in their resonant modes. This combination of attributes translates into opportunities for a number of important technological applications—such as ultrasensitive sensors,[4] and electromechanical signal processing components.[5] From a fundamental science point of view, NEMS might allow direct demonstrations of quantum mechanical phenomena.[6,7]

One of the central obstacles in front of developing NEMS based technologies, as well as access to interesting experimental regimes, is the realization of broadband and robust displacement detection methods with subnanometer resolution. Optical interferometry techniques, in particular path-stabilized Michelson interferometry and Fabry-Perot interferometry, are natural candidates for use in the domain of NEMS given their demonstrated sensitivity and broadband operation.[8–10] Both Michelson and Fabry-Perot interferometry have recently been applied to displacement detection in NEMS operated at room temperature.[2,11,12] It is clear that near-field optical phenomena affect the sensitivity of both techniques in the NEMS domain where critical device dimensions are in the deep submicron.

In this letter, our main focus is to gain a clear understanding of the way optical interferometric displacement detection works in subwavelength NEMS. In our experiments, interesting diffraction effects emerged as the relevant NEMS device dimensions were reduced beyond the optical wavelength used. First, optical response due to cavities in the smallest, subwavelength NEMS coupled most strongly to the displacement of the devices. Second, *conventional* path-stabilized Michelson interferometry technique appeared to suffer a severe sensitivity loss. In both cases, the experimental results were tested against detailed numerical models of the experiments.

The NEMS devices used in these experiments were silicon doubly clamped beams. The devices were fabricated on a silicon-on-insulator wafer with a 219-nm-thick silicon device layer on top of a 396-nm-thick sacrificial oxide layer. Figure 1(a) shows a scanning electron micrograph of a completed family of beams. There is a 40-nm-thick Cr metallization layer on top of the semiconductor device structures; the silicon substrate underneath is bare.

The optical measurements on fabricated devices were performed inside an ultrahigh vacuum (UHV) chamber through a quartz view port. Figure 1(b) displays the block diagram of the free-space optics employed. A He–Ne laser with wavelength, $\lambda \approx 632$ nm, was focused upon the center of a NEMS beam by a 50× objective lens with numerical aperture, NA=0.5. This resulted in an experimentally determined spot size (full width at half maximum) of 1.0 μm close to $\sim\lambda/2\text{NA}$. A schematic of the NEMS doubly clamped beam and the optical spot is displayed in Fig. 1(c).

First, we studied the properties of optical cavities in NEMS with emphasis on their use in displacement detection. The optical cavity is formed between the top surface of the metallized nanomechanical beam and the substrate as shown in Fig. 1(c). The intensity of the reflected light from such a cavity, hence, the resulting photodetector current, I depends upon the cavity length, z, and is usually measured by flexing the top layer towards the substrate electrostatically.[10] The relevant quantity for displacement detection in our setup is the z derivative of I, $\Re_C(w,z)=|\partial I(w)/\partial z|$, with units A/m. We shall call $\Re_C(w,z)$ the cavity displacement responsivity. In Fig. 2(a), we display $\Re_C$ for a 6.43 μm×600 nm ×219 nm ($l\times w\times t$) doubly clamped beam. We measured $\Re_C$ by inducing a small, off resonance ac displacement, δz, around a fixed cavity length, z, and determining the photodetector current variations, δI, from lock-in amplifier measurements. Both δz and z values were determined separately from Michelson interferometry on the same sample.

The solid line in Fig. 2(a) was obtained from a two-dimensional numerical model of the experiment. The two-dimensional approach, i.e., modeling the electromagnetic field variations around the cross section of the NEMS beam is a good approximation given that $l \gg w$ and $l \gg \lambda/2\text{NA}$ [see Fig. 1(c)]. In these computations, we determined[13] the electromagnetic field in the vicinity of a NEMS beam due to an

[a]Present address: Seoul National University of Technology, Seoul 139-743, Korea.
[b]Electronic mail: ekinci@bu.edu

 © 2005 American Institute of Physics
Downloaded 28 Dec 2004 to 128.197.50.37. Redistribution subject to AIP license or copyright, see http://apl.aip.org/apl/copyright.jsp

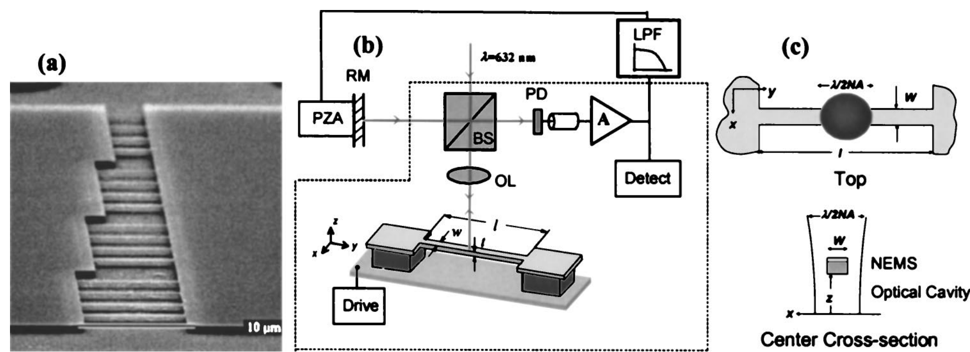

FIG. 1. (Color online) (a) Scanning electron micrograph of a family of doubly clamped silicon beams. The devices have the following dimensions, l, w, and t: 3 μm $< l <$ 10 μm, 150 nm $< w <$ 1000 nm, and t=219 nm; (b) schematic diagram of the free space optical setup. The main components used are beam splitter (BS), objective lens (OL), reference mirror (RM), photodetector (PD), broadband amplifier (A), low-pass filter (LPF), piezoelectric actuator (PZA). The dashed line indicates the portion of the setup used for the cavity measurements; the reference arm of the optics was used for the path-stabilized Michelson interferometry; (c) top view and center cross section of a doubly clamped NEMS beam in relation to the optical spot with Gaussian profile.

incoming transverse electric field with a Gaussian profile along the z direction. The Gaussian profile in the model approximated the experimental profile closely. We then computed the reflected power for varying beam-substrate gap (cavity length) values, z. Material properties were used for both Si and Cr layers in the NEMS device in order to obtain the complex permittivity values as $\varepsilon_{\mathrm{Si}} \approx 15.2-0.12i$ and $\varepsilon_{\mathrm{Cr}} \approx -92-61.4i$, respectively. The amplitude of the numerical data was normalized to fit the experimental data. In the inset of Fig. 2(a), we display a representative field distribution cross section [see Fig. 1(c)] of our 6.43 μm $\times$ 600 nm $\times$ 219 nm doubly clamped beam at a gap, z=200 nm. Both experimental and numerical results in Fig. 2(a) indicate that $\Re_C$ exhibits two maxima. The slight apparent mismatch between the experimental and numerical results, especially at small cavity lengths, might be due to the experimental error in displacement estimation or onset of elastic nonlinearities in the beam.

Next, we exploited the above-described cavity effect to transduce electromechanical NEMS resonances in the 10 MHz $< \omega/2\pi <$ 60 MHz range. In an effort to quantify the displacement sensitivity offered by the technique, we extracted $\Re_C(w,z)$ at (fixed) z=400 nm for a number of devices as a function of decreasing NEMS beam width, w. Our results are summarized in Fig. 2(b). The *inset* in Fig. 2(b) displays the on-resonance photodetector response from a family of four NEMS beams with *identical* lengths and thicknesses but *different* widths—vibrating at *exactly* the same rms amplitude. These beams with dimensions l =6.4 μm, t=219 nm, and varying w=1200, 600, 250, and 170 nm have resonance frequencies around $\omega_0/2\pi \sim$ 24 MHz with small variations of $\Delta\omega_0/\omega_0 \sim 1\%$; the mechanical Q factor variations in the beams have been taken into account. A very interesting effect is apparent: the displacement in the *smallest* device appears to couple *most strongly* to the optical response. The same effect is manifest in the more extensive $\Re_C$ vs. w data of Fig. 2(b). For each data point, i.e., doubly clamped beam with width, w, $\Re_C$ was extracted from resonance curves as $\Re_C \approx I(\omega_0)/z(\omega_0)$ with on-resonance photodetector current, $I(\omega_0)$, and displacement, $z(\omega_0)$. As w is increased to $w > \lambda/2\mathrm{NA}$, $\Re_C$ gets smaller. This is consistent with our expectations since the Cr film is essentially nontransparent. On the other end, as w is gradually reduced beyond the optical spot size, $\Re_C$ increases. Our attempts to model the w dependence of $\Re_C$ were relatively unsuccessful. A size dependent $\Re_C$, which increased with decreasing w, emerged from our simulations (not shown). However, the rise in the simulated $\Re_C$ with decreasing w was an *order of magnitude* larger than the experimentally observed one. This might be due to unaccounted-for losses in the experiments.

The displacement sensitivity (noise floor) per unit bandwidth attainable in our experimental setup at a given beam w by this technique depends upon $\Re_C(w,z)$ and the dominant noise source.[14] The latter was set by the current fluctuations in our broadband amplifier with (white) spectral density, $\sqrt{S_I} \approx 7$ pA/$\sqrt{\mathrm{Hz}}$. For our gap bias of $z \approx 400$ nm, the obtainable displacement sensitivity is $\sqrt{S_z} \approx \sqrt{S_I}/\Re_C(w)$, shown in Fig. 2(c). We note that using this technique even better $\sqrt{S_z}$ can be obtained by biasing the cavity at $z \approx z_0$ where $\Re_C(w,z)$ is maximized. For the w=600 nm beam of Fig. 2(a), for instance, biasing the gap around the points $z_0 \sim 80$ nm and $z_0 \sim 330$ nm would enable the most sensitive displacement detection.

We now turn to *conventional* path-stabilized Michelson interferometry technique in NEMS. In our experiments [Fig. 1(b)], the optical beam reflecting from the device which, in essence, is an optical cavity (see above discussion) interfered with the reference beam upon the photodetector. To clearly demonstrate the limits of path-stabilized Michelson interferometry, we have subtracted the above-quantified cavity effects from our results. Figure 3(a) shows the displacement responsivity of the Michelson interferometer, $\Re_M(w) = |\partial I(w)/\partial z|$, as a function of the NEMS beam width, w. We extracted $\Re_M$ in the following manner: we first carefully determined the *resultant* resonance responsivity [Fig. 3(a) inset], $\Re_{M+C} \approx I(\omega_0)/z(\omega_0)$, for each data point (device) and then subtracted the *cavity* responsivity from the resultant, $\Re_M \approx \Re_{M+C} - \Re_C$. We note that physically, this corresponds to taking away the substrate; such NEMS devices have been fabricated using silicon nitride membranes.[6] The solid line in Fig. 3(a) which we shall call $\alpha_\lambda(w)$ is the result of a numerical model. Here, the substrate surface was modeled as perfectly transmissive, essentially removing the cavity effects. $\Re_M(w)$ is well-described by this model and the earlier complications in modeling due to the substrate appear to have been resolved.

Clearly, diffraction effects have to be incorporated into the analysis. The electric field returning from the device to the photodetector will have the form $E_0\alpha_\lambda(w)e^{-ik(z_0-2\delta z)}$; the reference beam will be $E_R e^{-ikz_R}$ each with respective ampli-

Downloaded 28 Dec 2004 to 128.197.50.37. Redistribution subject to AIP license or copyright, see http://apl.aip.org/apl/copyright.jsp

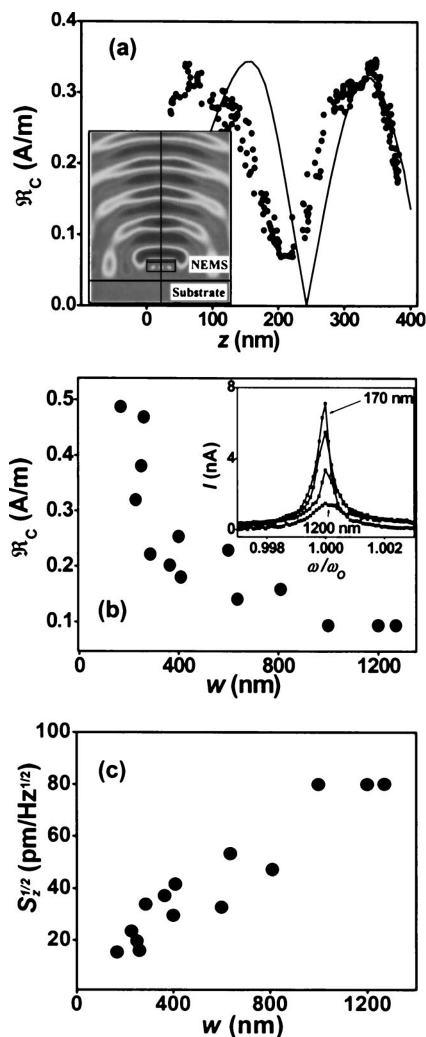

FIG. 2. (Color online) (a) The displacement responsivity, $\Re_C$, as a function of optical cavity length, z, for a Si doubly clamped beam with dimensions 6.43 μm $\times$ 600 nm $\times$ 219 nm. The solid line was generated from numerical models of the electromagnetic field as the beam was flexed towards the substrate—simulating the experiment. The color map in the inset shows the normalized electric field magnitude, E_y, around the center of the NEMS beam for $z=200$ nm; (b) displacement responsivity, $\Re_C$, as a function of w. The inset shows the resonance response from NEMS beams with *identical* lengths and thicknesses of $l=6.4$ μm, $t=219$ nm but *different* widths of $w=1200$, 600, 250, and 170 nm. The beams are vibrating at *exactly* the same rms amplitude. The photodetector current signal, I, is largest for the beam with the smallest w and decreases with increasing w; (c) displacement sensitivity per unit bandwidth, $\sqrt{S_z}$, as a function of w obtainable by exploiting the optical cavity effects in NEMS. The current noise in our broadband amplifier was the dominant noise source.

tudes E_0 and E_R. Here, z_R represents the total path traversed by the reference beam; z_0 represents the static portion of the total path of the object beam to detector; δz is the dynamic path variation. The change in the photodetector current, $\delta I(w)$, due to the intensity variation at the photodetector will be proportional to $E_R E_0 \alpha_\lambda(w)\delta z$ for $\delta z \ll \lambda$. This clearly indicates that $\Re_M(w) \propto \alpha_\lambda(w)$, as verified experimentally. Consequently, our displacement sensitivity per unit bandwidth decreases (noise floor increases) as a function of decreasing w,

$$\sqrt{S_z} \approx \sqrt{S_I}/\Re_M(w) \propto 1/\alpha_\lambda(w).$$

Given that $\sqrt{S_I} \approx 7$ pA/$\sqrt{\text{Hz}}$, we have plotted the displacement sensitivity (noise floor) as a function of NEMS width,

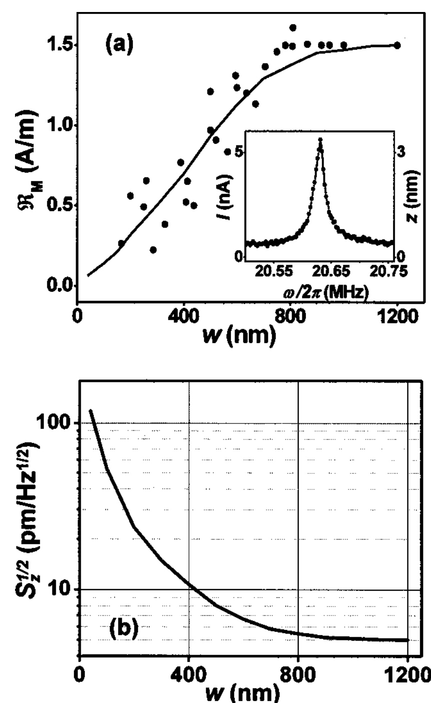

FIG. 3. (a) Displacement responsivity of our path stabilized Michelson interferometer, $\Re_M$, as a function of w. The inset shows the resonance line shape for a beam with dimensions, 8.5 μm $\times$ 900 nm $\times$ 219 nm, and $\omega_0/2\pi \approx 20$ MHz. The solid line is the result of a numerical model; (b) Displacement sensitivity per unit bandwidth, $\sqrt{S_z}$, as a function of w in our conventional path-stabilized Michelson interferometer.

w, achievable by our Michelson interferometer in Fig. 3(b).

In summary, our measurements and calculations show conclusively that as the relevant NEMS dimensions are reduced beyond the optical wavelength used, diffraction effects dominate the workings of optical displacement detection techniques. There is a clear need to explore optical near-field techniques in next generation, smaller NEMS applications.

The authors gratefully acknowledge support from the NSF under Grant Nos. 210752, 216274, and 324416. The authors would like to thank Dr. T. W. Murray, Dr. S. B. Ipppolito, Dr. B. B. Goldberg, and Dr. M. S. Ünlü for many helpful discussions.

[1]M. L. Roukes, Phys. World **14**, 25 (2001).
[2]D. W. Carr, S. Evoy, L. Sekaric, H. G. Craighead, and J. M. Parpia, Appl. Phys. Lett. **75**, 920 (1999).
[3]M. Blencowe, Phys. Rep. **395**, 159 (2004).
[4]K. L. Ekinci, X. M. H. Huang, and M. L. Roukes, Appl. Phys. Lett. **84**, 4469 (2004).
[5]A. Erbe, H. Krömmer, A. Kraus, R. H. Blick, G. Corso, and K. Richter, Appl. Phys. Lett. **77**, 3102 (2000).
[6]M. D. LaHaye, O. Buu, B. Camarota, and K. C. Schwab, Science **304**, 74 (2004).
[7]R. G. Knobel and A. N. Cleland, Nature (London) **424**, 291 (2003).
[8]J. W. Wagner, Phys. Acoust. **19**, 201 (1990).
[9]J. V. Knuuttila, P. T. Tikka, and M. M. Salomaa, Opt. Lett. **25**, 613 (2000).
[10]R. L. Waters and M. E. Aklufi, Appl. Phys. Lett. **81**, 3320 (2004).
[11]C. Meyer, H. Lorenz, and K. Karrai, Appl. Phys. Lett. **83**, 2420 (2003).
[12]B. E. N. Keeler, D. W. Carr, J. P. Sullivan, T. A. Friedmann, and J. R. Wendt, Opt. Lett. **29**, 1182 (2004).
[13]We used finite element analysis to determine the electromagnetic fields.
[14]The use of extremely low optical power levels, $P \sim 50$ μW, did not allow shot noise limited operation.

Downloaded 28 Dec 2004 to 128.197.50.37. Redistribution subject to AIP license or copyright, see http://apl.aip.org/apl/copyright.jsp